JOURNAL OF MATERIALS SCIENCE **36** (2001) 5767 – 5772

High temperature deformation behavior of crystallized precursor-derived Si-B-C-N ceramics

MARTIN CHRIST, ANDRÉ ZIMMERMANN, ACHIM ZERN, MARKUS WEINMANN, FRITZ ALDINGER
Max-Planck-Institut für Metallforschung and Institut für Nichtmetallische Anorganische Materialien, Universität Stuttgart, Pulvermetallurgisches Laboratorium, Heisenbergstrasse 5, D-70569 Stuttgart, Germany
E-mail: zimmermann@mf.mpg.de

Annealing of amorphous precursor-derived Si-B-C-N ceramics for 3 h at 1800°C in 15 bar nitrogen yielded a material consisting of SiC with a mean grain size of about 100 nm, embedded in a turbostratic B-C-N phase. The deformation behavior of this material was investigated by compression tests at 1400°C in air. Dependent on the applied stress the strain rate decreased with time. The deformation rate consists of a stress dependent component that is proportional to the applied stress, which indicates that this part of the deformation mechanism is based on viscous flow. Furthermore, the influence of oxidation on the deformation behavior is investigated.

1. Introduction

Precursor-derived covalent ceramics based on silicon, boron, carbon and nitrogen (Si-B-C-N) proved to posess high thermal [1–4], chemical [5] and mechanical [6] stability due to the lack of oxidic grain boundary phases. Detailed studies on the mechanical properties of as-thermolysed Si-C-N [7, 8] and Si-B-C-N [9–11] materials revealed an outstanding mechanical stability of the amorphous state at rather high temperatures. It has been shown, that the plastic deformation consists of a stress-dependent and a stress-independent component [7, 11]. The first component is proportional to the applied stress [7, 8, 11, 12] and is assumed to be caused by plastic flow, while the second one can be ascribed to shrinkage [11]. The plastic behavior of the amorphous ceramics could be explained by a deformation model, which has been developed for metallic glasses. According to this model [13, 14], materials flow is based on structural defects consisting of deviations from the "ideal" amorphous structure, i. e. fluctuations in the free volume distribution.

During post-annealing of as-thermolysed materials, the free volume heals out partially leading to a decrease of the specific volume and a decrease of the flow defect concentration and thus to an increase of the viscosity of the amorphous material.

To our knowledge, no detailed investigations of the mechanical high-temperature properties of crystalline precursor-derived ceramics are published until now. This paper reports on crystallization experiments of Si-B-C-N ceramics and their mechanical behavior at high temperature under compression.

2. Experimental procedure

The ceramics investigated here were derived from a boron-modified polyvinylsilazane (MW33) with the idealized molecular structure $\{B[C_2H_4\text{-}Si(H)NH]_3\}_n$ [5]. Polymer synthesis yielded a brittle and unmeltable product. For further processing, the polymer was ground using a vibrating-disk mill and sieved to particle sizes smaller than 32 μm. For compaction the polymer powder was heated in a graphite die up to a temperature of about 350°C, where the polymer softens, and subsequently densified by an uniaxial pressure of 48 MPa. The green bodies obtained were converted into amorphous ceramic monoliths via thermolysis in an argon atmosphere by heating with a heating rate of 1°C/min and subsequent annealing for 2 h at 1400°C.

For crystallization, the as-thermolysed ceramics were further annealed in nitrogen atmosphere (15 bar) at 1800°C for 3 h in boron nitride crucibles. The applied heating and cooling rates were 10°C/min. To monitor the density change of the pore-free ceramics during the crystallization process, amorphous MW33-derived ceramic powder with a particle size smaller than 32 μm was annealed in the same run. The density ρ_p of the powder was measured by helium gas pycnometry and the bulk density ρ_{bulk} of the ceramics by submersion of the specimen in mercury using the Archimedes principle. The crystallization was investigated by XRD and TEM. Electron spectroscopic imaging (ESI) was used to detect the lateral distribution of the elements. Furthermore, the chemical composition of the specimen was determined before and after the crystallization by elemental analysis. The concentration of nitrogen and oxygen was determined by carrier gas hot extraction. The concentration of silicon and boron was determined by Fourier-transformation infrared spectrometry (Fluorine Volatilization-FTIRS) and optical emission spectrometry with an inductively coupled plasma (ICP-OES) [15].

From the crystallized samples, specimen with a height of 3 mm and a cross sectional area of

1.8×1.8 mm^2 were prepared. The high temperature mechanical behavior was investigated by compression tests in air at 1400°C. The mechanical testing equipment is described elsewhere [7].

3. Results

3.1. Crystallization

According to the XRD-data presented in Fig. 1, the as-thermolysed ceramics are amorphous. In contrast, the diffraction pattern of the annealed samples exhibits sharp peaks that can be ascribed to the 6h-SiC phase. TEM studies revealed a microstructure consisting of crystallites with a mean grain size of about 100 nm embedded in a turbostratic grain boundary phase (Fig. 2). The distribution of silicon, boron, carbon and nitrogen determined by ESI is shown in Fig. 3. In the bright regions, the concentration of the particular element is increased. There is no indication for Si_3N_4 crystallites to be present. The dark regions in the silicon map coincide with the turbostratic grain boundary phase. Thus, in agreement with the XRD results, the crystallites consist of silicon and carbon. The grain boundary phase contains boron, carbon and nitrogen. By a quantitative analysis of the atomic ratios, the constitution of the grain boundary phase is determined to be C:B:N = 1:1:1.

This is in accordance with results of the elemental analysis of the as-thermolysed and the annealed ceramics as listed in Table I. As-thermolysed material contains a fraction of 30.0 at.% nitrogen, which decreases during crystallization to about 12 at.%, whereas the amount of the other elements increases proportional. Taking into account the findings depicted in Figs 2 and 3 and considering that all silicon is bonded as silicon carbide, the calculated C:B:N element ratio in the turbostratic phase is 0.8:1:1. Table II shows the results of the pycnometric and porosimetric characterization of the crystallized sample. Even though the density ρ_p of the crystallized powder is increased with respect to that of the as-thermolysed material, its porosity is higher. In the thermodynamic equilibrium, an MW33-derived crystalline ceramic would consist of 21.7 wt% graphite ($\rho = 2.25$ g/cm^3), 32.5 wt% silicon nitride ($\rho = 3.20$ g/cm^3), 14.0 wt% boron nitride ($\rho = 2.27$ g/cm^3) and 31.8 wt% silicon carbide ($\rho = 3.20$ g/cm^3) [5]. Using the rule of mixtures, the calculated density of a crystalline material with this composition would be $\rho_{cryst} = 2.8$ g/cm^3, compared to the measured density of 2.40 g/cm^3 of the as-thermolysed material. The powder density ρ_p of both specimen was below this value. To quantify the deviation of the actual powder density from the maximum value ρ_{cryst}, the density deficit δ of the powder density in comparison to the calculated maximum value is used:

$$\delta = 1 - \rho_p/\rho_{cryst} \tag{1}$$

TABLE I Chemical composition of as-thermolysed and crystallized MW33-derived ceramics. The oxygen content was below 2.0 wt%

	As thermolysed			After crystallization		
	Analysis	Standardized		Analysis	Standardized	
	(wt%)	(wt%)	(at.%)	(wt%)	(wt%)	(at.%)
Si	42.8	43.7	26.0	52.4	53.6	33.4
B	5.7	5.8	9.0	7.0	7.2	11.7
C	24.7	25.2	35.0	28.5	29.2	42.6
N	24.7	25.2	30.0	9.8	10.0	12.3
Summation	97.9	100.0	100.0	97.7	100.0	100.0

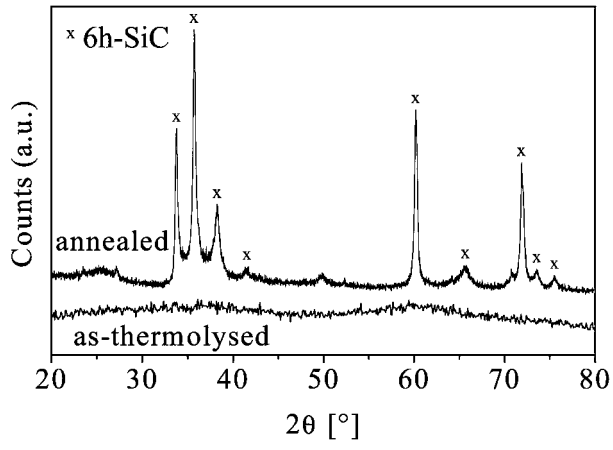

Figure 1 XRD diffraction pattern of as-thermolysed (1400°C, 2 h, 1 bar Ar) and annealed (1800°C, 3 h, 15 bar N_2) MW33-derived ceramics. The diffraction pattern of the annealed sample indicates the occurrence of 6h-SiC.

TABLE II Comparison of the pycnometric data of the as-thermolysed and the annealed samples. The density deficit δ is calculated according to Equation 1

	Porosity (%)	ρ_{bulk} (g/cm^3)	ρ_p (g/cm^3)	δ(%)
As thermolysed	16	2.02	2.40	14
Annealed	21	2.05	2.59	7.5

3.2. Deformation behavior

With the crystallized MW33-derived material, a stress change compression experiment was performed at 1400°C. The dependency of the total strain and that of the strain rate $\dot{\varepsilon}$ on the time is plotted in Fig. 4. After more than 50 h under constant load, the strain rate still decreases continuously without approaching a constant value. As in the case of amorphous precursor-derived ceramics [11, 12], the strain rate of the crystallized material can be approximated by a equation of the form

$$\dot{\varepsilon} = \frac{1}{(a + b \cdot t)}, \tag{2}$$

where t represents the time, and a and b are constants. The lines in Fig. 4 provide a fit of Equation 2 to the data measured for 100 MPa and 200 MPa, respectively. Differences between the fitted lines and the measured data are likely caused by anelastic behavior, which is also observed in amorphous precursor-derived ceramics [16]. According to the conventional definition, the term anelastic denotes the reversible and time dependent deformation [17]. Although the deformation behavior is qualitatively the same for crystallized and amorphous materials, the strain rate of the crystallized ceramics at 100 MPa and 1400°C amounts only to about 20% of the strain rates, that are observed for amorphous material under the same conditions. To determine the

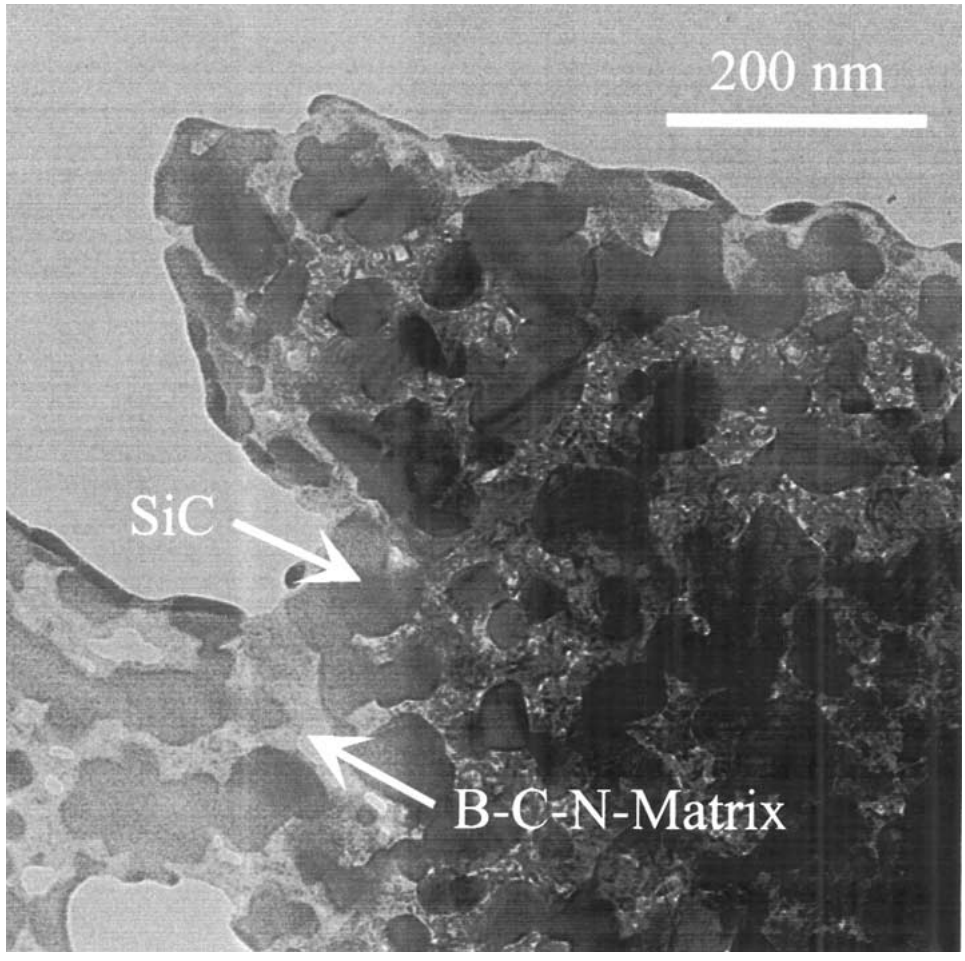

Figure 2 TEM-micrograph of an annealed (1800°C, 3 h, 15 bar N_2) MW33-derived ceramic. The microstructure consists of SiC crystals (dark) of a mean grain size of about 100 nm embedded in a matrix of turbostratic B-C-N. The distribution of silicon, boron, carbon and nitrogen is shown in Fig. 3.

stress dependency, the strain rates measured at 100 MPa and 200 MPa, respectively, are extrapolated to $t = 10^6$ s and compared with the strain rate measured at this time under 150 MPa. Therefore, Equation 2 is fitted to the measured data using the least-squares method. In Fig. 5 the strain rate is plotted as a function of the applied stress. As for amorphous precursor-derived ceramics [11, 12], the data can be represented by an affine linear function:

$$\dot{\varepsilon} = A + B \cdot \sigma \tag{3}$$

where A and B are constants and σ represents the stress. The linear relation between the stress and the stress dependent component of the strain rate are hints for a deformation mechanism based on viscous flow. Thus it is justified to derive the Newtonian viscosity η of the material from the parameter B in Equation 3:

$$\eta = \frac{1}{(3 \cdot B)}$$

This leads to a value of $\eta_{\text{cryst}}(10^6 \text{ s}, 1400°\text{C}) = 4.0 \times 10^{15}$ Pa s, which is in the same order of magnitude as the viscosity of amorphous Si-B-C-N ceramics under the same conditions [11, 12]. However, in this case the stress independent component of the deformation rate has a negative value. This means, that the specimen expands at high temperatures in air without external load.

4. Discussion

4.1. Crystallization

During the annealing of amorphous precursor-derived ceramics, the powder density ρ_p increases. This can be explained by the reduction of free volume [11]. The powder density of the crystallized ceramic is increased as well with respect to the as-thermolysed state, although the calculated density $\rho_{\text{cryst}} = 2.8$ g/cm^3 is not reached. The remaining density deficit of about 7.5% is likely due to the distortion of the turbostratic B-C-N phase. This amount of free volume is still significantly higher than the value of about 2.5%, that is usually observed in super-cooled melts at the glass transition temperature [18].

The significantly lower nitrogen content of the annealed material as compared to the as-thermolysed ceramics shows that crystallization is associated with decomposition. This is in contradiction to [5], where it is reported for MW33-derived ceramic powders, that crystallization occurs at about 1700°C, whereas decomposition is observed only at about 2000°C. This difference in the high temperature stability between ceramic powders and ceramic monoliths is most probably caused by the processing. It was shown recently, that the decomposition temperature of MW33-derived ceramic powder decreases with decreasing powder

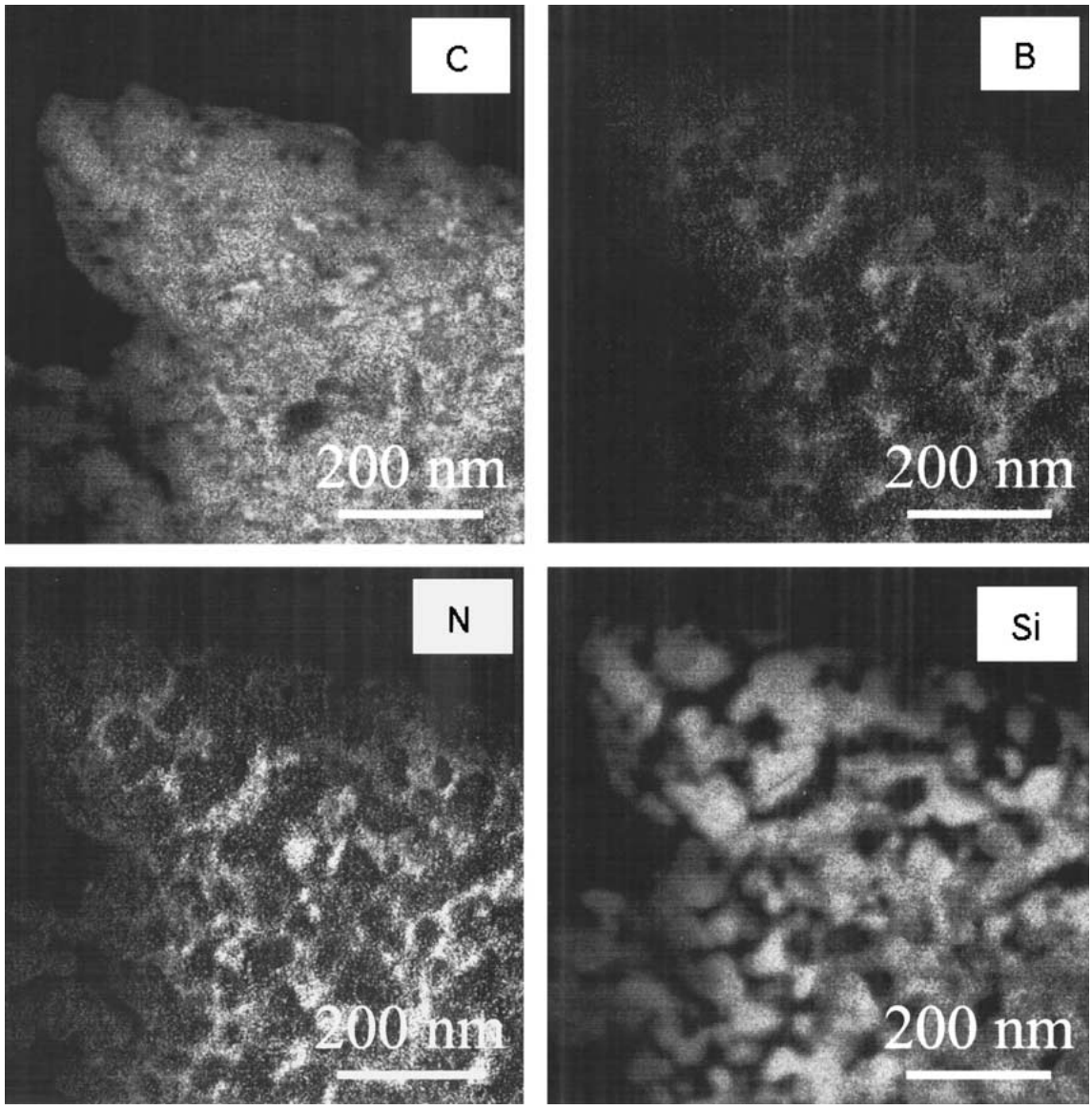

Figure 3 Elemental distribution images of a crystallized MW33-derived ceramic. A bright field image of the sample is shown in Fig. 2.

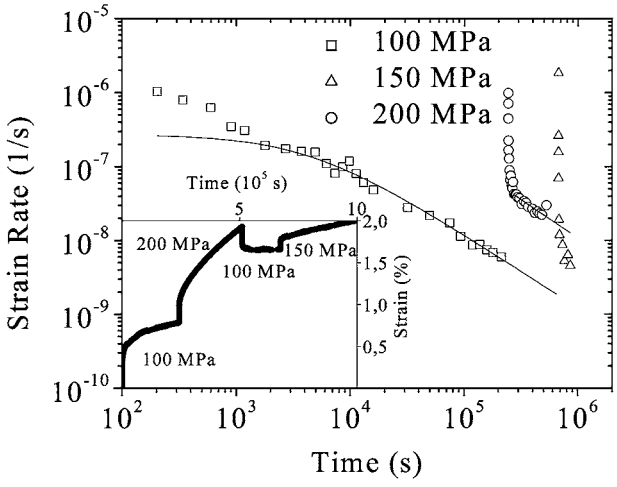

Figure 4 Compression test of crystallized MW33-derived ceramic at 1400°C in air and different stresses. The line represents a fit of Equation 2 to the data. In the inset, the total strain is plotted as a function of the time.

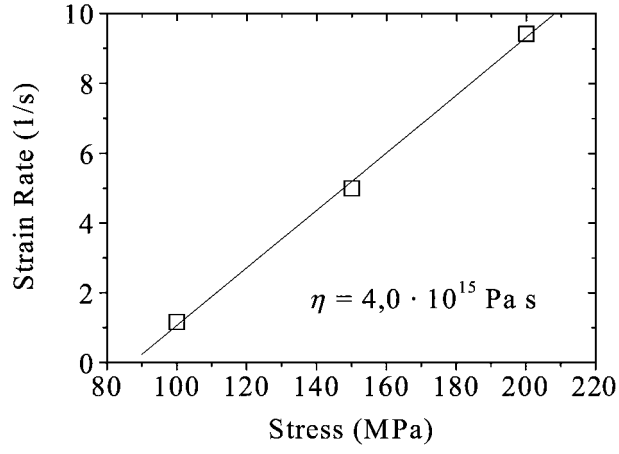

Figure 5 Strain rate of a crystallized MW33-derived sample after 10^6 s at different stresses. The values for 100 MPa and 200 MPa are extrapolated from shorter times using Equation 2. From the slope of the fitted line the viscosity η can be determined.

particle size [19]. This can be checked by measuring the weight loss of powder samples during annealing in inert gas atmosphere. For a particle size larger than 315 μm a decomposition temperature of more than 2000°C was observed, whereas a powder with a particle size between 32 μm and 80 μm decomposes at about 1700°C [19]. As the samples investigated in this work have been fabricated from polymer powder with a particle size

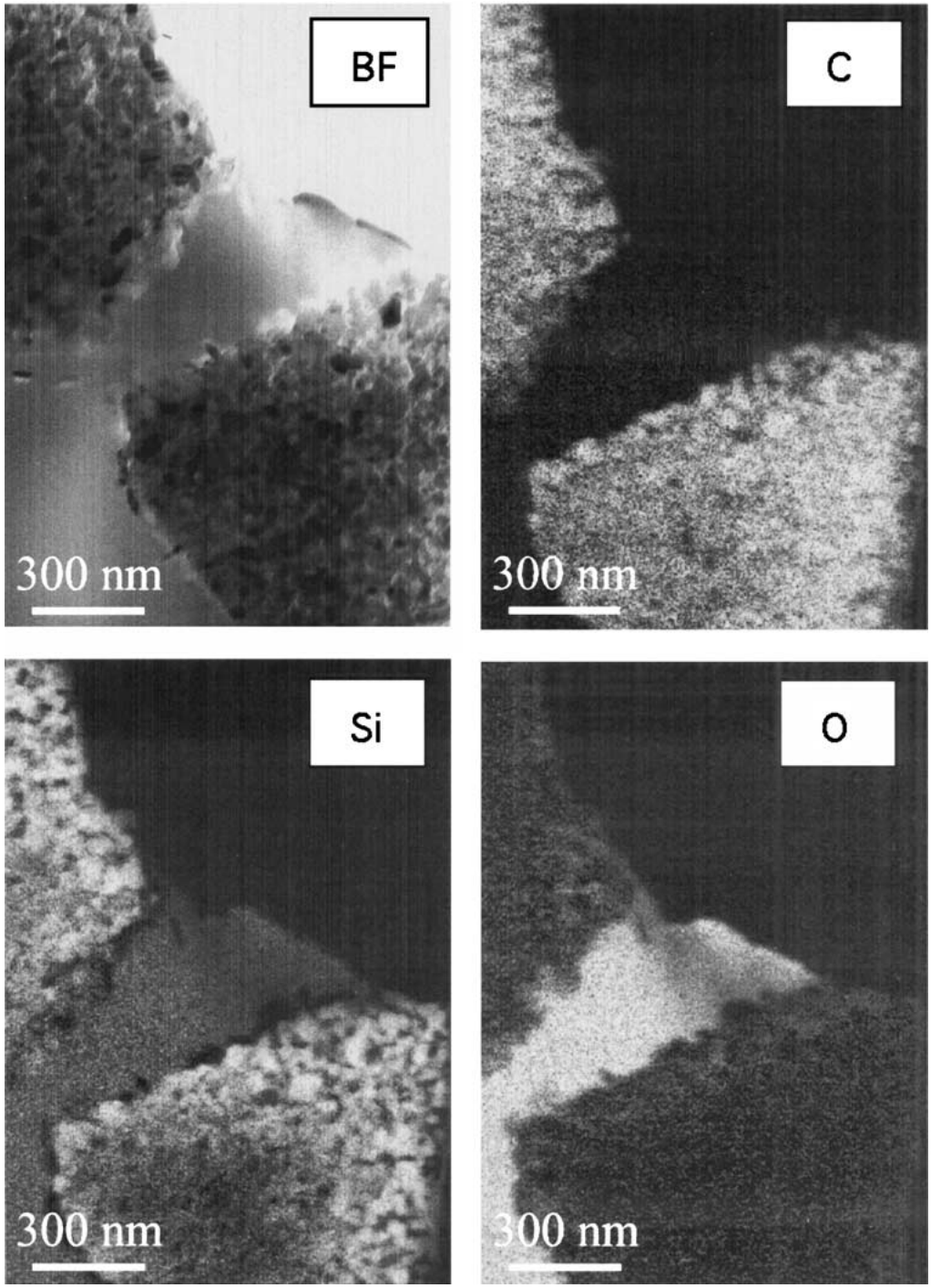

Figure 6 TEM bright field image and distribution images of carbon, silicon and oxygen inside a crystallized MW33-derived ceramic after compression loading at 1400°C for 310 h in air.

smaller than 32 μm it is hypothesized that their decomposition temperature is lowered with respect to material derived from the as received polymer.

4.2. Deformation and oxidation behavior

The high temperature deformation behavior of crystallized precursor-derived ceramics is similar to that observed for amorphous materials. The plastic deformation consists as well of two components, one being independent of the applied stress and the other being proportional to the applied stress. The latter component shows the same time dependence as it is observed for amorphous materials. This might be explained by the occurance of the turbostratic B-C-N phase consisting of hexagonal layers with fluctuations of the inter-layer distance [3, 20]. Thus, this phase can be more easily deformed than the SiC crystallites. Similarly, the deformation behavior of liquid phase sintered SiC and Si_3N_4 ceramics consisting of rigid crystallites and a matrix with a lower viscosity is known to be determined by the properties of the matrix [21]. The lack of a long-range order in the turbostratic phase of MW33-derived crystallized ceramics apparently leads to a deformation behavior similar to that of the amorphous material. Thus, the time dependence of the deformation rate might be explained by the annealing out of defects from the turbostratic B-C-N phase.

The strain component of the crystallized MW33-derived ceramics which is independent of the applied

stress differs significantly from that of the amorphous material. Whereas the volume of the latter one decreases at high temperature due to the annealing out of free volume, the crystallized material expands during exposure to high temperatures in air. This might be caused by oxidation. In contrast to amorphous precursor-derived ceramics which form a passivating oxide layer on the surface, the crystallized ceramics investigated in this work show oxidation inside the specimen. Fig. 6 shows a bright field image and element maps of silicon, carbon and oxygen taken by TEM from a MW33-derived crystallized specimen after a compression test at 1400°C for 310 h in air. In the bright field image, two former polymer particles are visible which have been converted into a crystalline ceramic with a nano-scale microstructure. According to the elemental distribution images, the light-gray, featureless area in between of the two former polymer particles consists of silicon and oxygen. Thus it is likely that in the crystallized specimen under investigation oxidation takes place mainly at the boundaries between the former polymer particles. This incorporation of oxygen could explain the volume increase during exposure to air at high temperatures. For comparison, in Figs 2 and 3 TEM images of the microstructure before the compression test are shown.

The different oxidation behavior of crystallized and amorphous ceramics might be a consequence of the decomposition processes during crystallization. As shown in Table II, the porosity and thus the surface of the annealed sample is increased with respect to the as-thermolysed state. Furthermore, a loss of nitrogen is observed after annealing. The pathways of the gaseous decomposition products can also serve as such for oxygen.

5. Conclusions

Si-B-C-N precursor-derived ceramics were crystallized by annealing at 1800°C for 3 h in 15 bar nitrogen. According to TEM and XRD investigations, the resulting microstructure consisted of 6h-SiC grains with a mean size of about 100 nm, embedded in a turbostratic B-C-N phase. The crystallization of the material was accompanied by decomposition and a loss of nitrogen. The deformation behavior of the crystallized material under compression in air at 1400°C is characterized, as it was observed for amorphous precursor-derived ceramics, by a continuous decrease of strain rate with time. The plastic deformation consists of a stress independent component that can be explained by the incorporation of oxygen and a second component which is proportional to the applied stress giving a hint for a deformation mechanism based on viscous flow of the turbostratic B-C-N phase.

The decomposition accompanying crystallization and the oxidation behavior observed in this work are assumed to be not intrinsic properties of precursor-derived ceramics but are likely caused by the processing. Therefore, future efforts have to be concerned with improvements with respect to the processing.

Acknowledgement

The authors thank the Deutsche Forschungsgemeinschaft for financial support and Mr. R. Mager for the preparation of the creep specimens and technical support.

References

1. R. RIEDEL, A. KIENZLE, W. DRESSLER, L. M. RUWISCH, J. BILL and F. ALDINGER, *Nature* **382** (1996) 796.
2. J. BILL and F. ALDINGER, *Adv. Mater.* **7**(9) (1995) 775.
3. H.-P. BALDUS and M. JANSEN, *Angew. Chem. Int. Ed. Engl.* **36** (1997) 328.
4. M. WEINMANN, T. W. KAMPHOWE, J. SCHUMACHER, K. MÜLLER and F. ALDINGER, *Chem. Mater.* **8** (2000) 2112.
5. M. WEINMANN, J. SCHUHMACHER, H. KUMMER, S. PRINZ, J. PENG, H. J. SEIFERT, M. CHRIST, K. MÜLLER, J. BILL and F. ALDINGER, *ibid.* **12** (2000) 623.
6. G. THURN and F. ALDINGER, in Proceedings of the International Workshop on Grain Boundary Dynamics of Precursor-Derived Covalent Ceramics, Schloß Ringberg, 1996, edited by J. Bill, F. Wakai, and F. Aldinger (Wiley-VCH, Weinheim, Germany, 1999) p. 237.
7. G. THURN, J. CANEL, J. BILL and F. ALDINGER, *J. Eur. Ceram. Soc.* **19**(13/14) (1999) 2317.
8. L. AN, R. RIEDEL, C. KONETSCHNY, H.-J. KLEEBE and R. RAJ, *J. Amer. Ceram. Soc.* **81**(5) (1998) 1349.
9. B. BAUFELD, H. GU, J. BILL, F. WAKAI and F. ALDINGER, *J. Eur. Ceram. Soc.* **19** (1999) 2729.
10. R. RIEDEL, L. M. RUWISCH, L. AN and R. RAJ, *J. Amer. Ceram. Soc.* **81**(12) (1998) 3341.
11. M. CHRIST, G. THURN, M. WEINMANN, J. BILL and F. ALDINGER, *ibid.* **83** (2000) 3025.
12. M. CHRIST, G. THURN, J. BILL and F. ALDINGER, in "Ceramics—Processing, Reliability, Tribology and Wear, Euromat," edited by G. Müller (Wiley-VCH, Weinheim, Germany, 2000) p. 359.
13. M. H. COHEN and D. TURNBULL, *J. Chem. Phys.* **31** (1959) 1164.
14. F. SPAEPEN, in "Physics of Defects," Les Houches Lectures XXXV, edited by R. Balian, M. Kléman and J. -P. Poirier (North Holland, Amsterdam, 1981) p. 134.
15. G. KAISER, A. MEYER, M. FRIESS, R. RIEDEL, M. HARRIS, E. JACOB and G. TÖLG, *Fresenius J. Anal. Chem.* **352** (1995) 318.
16. M. CHRIST, A. ZIMMERMANN and F. ALDINGER, *J. Mater. Res.* **16** (2001) 1994.
17. N. G. McCRUM, "Anelastic and Dielectric Effects in Polymeric Solids" (Dover Publications, St. Mineola, 1991).
18. M. L. WILLIAMS, R. F. LANDEL and J. D. FERRY, *J. Amer. Chem. Soc.* **77** (1955) 3701.
19. J. NARAYANAN, Diploma thesis, University of Stuttgart, (2000).
20. A. JALOWIECKI, J. BILL and F. ALDINGER, *Composites Part A* **27A** (1996) 717.
21. W. E. LUECKE, S. M. WIEDERHORN, B. J. HOCKEY, R. F. KRAUSE JR. and G. G. LONG, *J. Amer. Ceram. Soc.* **78** (1995) 2085.

Received 9 January
and accepted 23 July 2001